GROUND STATE MANIFOLDS IN FRUSTRATED MAGNETS

Péter Kránitz

Physics BSc
Faculty of Natural Sciences
Budapest University of Technology and Economics

Supervisor:

Karlo Penc

Institute for Solid State Physics and Optics
Wigner Research Centre for Physics

October 2021

Abstract

The magnetic ions in pyrochlores (with chemical formula AB_2O_7, where A and B are metal ions) and in spinels (AB_2O_4) form the pyrochlore lattice constructed from corner-sharing tetrahedra. The pyrochlore lattice is highly frustrated, where the classical Heisenberg model remains disordered down to $T = 0$ temperature. Much less is known about the fate of the $S = 1/2$ spins. A recent numerical calculation provided evidence for the inversion symmetry breaking in the ground state of the quantum SU(2) symmetric Heisenberg model [1].

Inspired by these results, we construct a Hamiltonian with an exact ground-state manifold that breaks the inversion symmetry. In the ground state, the spins on one of the sublattices of the tetrahedra form singlets, and the wave function is a product of such singlets. Since each tetrahedron can support two linearly independent SU(2) singlets, the number of states in this highly degenerate ground state manifold is $2 \cdot 2^{N_{\text{tet}}/2}$, where N_{tet} is the number of tetrahedra.

To obtain the Hamiltonian, we consider a 7-site motif built from two corner-sharing tetrahedra. We require that the wave functions of spins forming a singlet in one of the tetrahedra are eigenstates of the motif Hamiltonian consisting of two- and four-spin exchanges. The Hamiltonian is then the sum over the motifs covering the lattice. We apply this construction to the checkerboard lattice, which is the 2-dimensional analog of the pyrochlore lattice. Numerical exact diagonalization of 16- and 20-site periodic clusters recovered the expected degeneracy of the ground state manifold. We also provide an exact lower bound for the energy of the checkerboard cluster.

Contents

Chapter 1

Introduction

1.1 Frustrated magnets

In a magnetic system, the interaction between the magnetic moments $\mathbf{M}_i$ is given by the Heisenberg model. Since the magnetic moments $\mathbf{M}_i$ are proportional to the spin $\mathbf{S}_i$ of the localized electrons, the Heisenberg Hamiltonian is written as

$$H = \frac{1}{2} \sum_{i,j} J_{i,j} \mathbf{S}_i \cdot \mathbf{S}_j \,, \tag{1.1}$$

where $\mathbf{S}_i$ is the spin operator at the site i in the lattice, and $J_{i,j} = J_{j,i}$ is the exchange interaction between $\mathbf{S}_i$ and $\mathbf{S}_j$. In the insulating magnetic systems, when the origin of the interaction is the superexchange, the $J_{i,j} > 0$ and the coupling is antiferromagnetic [2]. The $\mathbf{S}_i$ for a single localized electron is $S = 1/2$. Due to Hund's rule, several electrons can form larger spins, like $S = 3/2$ of the Cr^{3+} ions in the $CdCr_2O_4$ spinels, or $S = 5/2$ of the Fe^{3+} in the $ZnFe_2O_4$ [3]. For larger spins, the quantum effects can be neglected. Instead of the operators we can use three-component vectors $\mathbf{S}$ in Eq. (1.1), with magnitude $\mathbf{S}^2 = 1$, these are called classical spins.

For classical spins, the antiferromagnetic Heisenberg Hamiltonian on a single bond with $J_{i,j} > 0$ is minimized when $\mathbf{S}_i = -\mathbf{S}_j$. On bipartite lattices, such as the square and cubic lattice with nearest interactions only, the spins order antiferromagnetically – they form a two sublattice structure with antiparallel orientations. On every bond the classical energy is optimal, $\mathbf{S}_i \cdot \mathbf{S}_j = -1$. In non-bipartite lattices, such as triangular or other lattices containing triangles, the spins can't satisfy this condition.

Let us demonstrate this by a triangle with classical spins and Hamiltonian

$$H = J \left(\mathbf{S}_1 \cdot \mathbf{S}_2 + \mathbf{S}_1 \cdot \mathbf{S}_3 + \mathbf{S}_2 \cdot \mathbf{S}_3 \right) . \tag{1.2}$$

This Hamiltonian can be written as a full square:

$$H = \frac{J}{2} \mathbf{S}_{\text{tot}}^2 - \frac{3}{2} J \,, \tag{1.3}$$

where $\mathbf{S}_{\text{tot}} = \sum_{i=1}^{3} \mathbf{S}_i$. If two spins are parallel and the third spin is antiparallel to both of them, like in Fig. 1.1(a), the total energy is equal to $-J$. Instead, the total energy is minimal

when $\mathbf{S}_{\text{tot}} = 0$, so the spins enclose $120°$ and lay in the same plane, as in Fig. 1.1(b). In this case, the total energy is $-\frac{3}{2}J$. This is a *frustrated* system since neither of the bonds reaches the optimal energy $-J$. Let us note, that this state is unique, neglecting the trivial degeneracy due to global O(3) rotations.
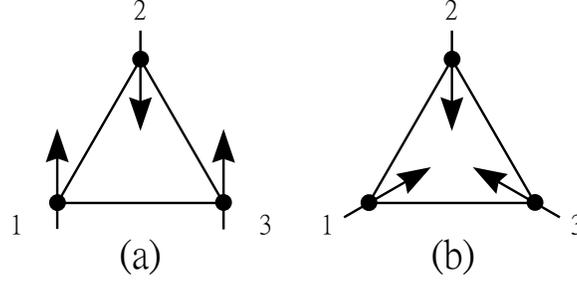

Figure 1.1: Classical spin configurations in the triangle. Arrows represent the classical spins. In (a), the energies of bonds 1,2 and 2,3 are optimal $(-J)$, but very bad on the bond 1,3 $(+J)$, the total energy of the configuration is $-J$. (b) Neither of the bond energies $(-J/2)$ are optimal, but this is the minimal energy configuration with $-3J/2$.

In the case of the tetrahedron, the Hamiltonian can be written in the form

$$H = J \sum_{1 \leqslant i < j}^{4} \mathbf{S}_i \mathbf{S}_j \ . \tag{1.4}$$

Like in the case of triangle, the Hamiltonian can be expressed.

$$H = \frac{J}{2} \mathbf{S}_{\text{tot}}^2 - 3J \ , \tag{1.5}$$

where

$$\mathbf{S}_{\text{tot}} = \mathbf{S}_1 + \mathbf{S}_2 + \mathbf{S}_3 + \mathbf{S}_4. \tag{1.6}$$

We will refer to the equation as the tetrahedron rule. The total energy is minimized when $\mathbf{S}_{\text{tot}} = 0$, but instead of a unique state (as for triangle), now we have an infinite number of configurations because now the spins have two internal degrees of freedom to find appropriate configuration, as illustrated in Fig.1.2 [4].
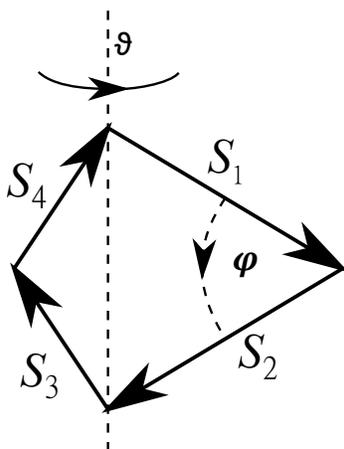
Figure 1.2: The two degrees of freedom ϑ and φ for classical spins on a tetrahedron satisfying the $\mathbf{S_1} + \mathbf{S_2} + \mathbf{S_3} + \mathbf{S_4} = 0$ condition.

The tetrahedra are the building blocks of the pyrochlore lattice which is constructed from corner-sharing tetrahedra. The pyrochlore lattice is realized by the magnetic ions (B) in pyrochlores with chemical formula $A_2B_2O_7$, where A and B are metal ions, and in AB_2O_4 spinels. The classical spins in the pyrochlore lattice inherit the large degeneracy of the ground state of a tetrahedron: An extensively degenerate ground state manifold will satisfy the $\mathbf{S}_{\mathrm{tot}} = 0$ condition for each tetrahedron in the lattice.

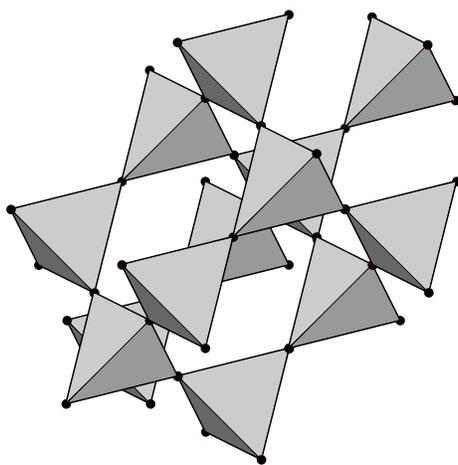Figure 1.3: Pyrochlore lattice built-up of corner-sharing tetrahedra.

An explicit construction of the ground state for pyrochlore lattice with n-component classical spin shows that the correlation function for Heisenberg spins, which gives the collinearity of the spin system, gives zero over two nearest-neighbor distances, even at very low temperatures, confirming the vast degeneracy of the pyrochlore lattice [5].
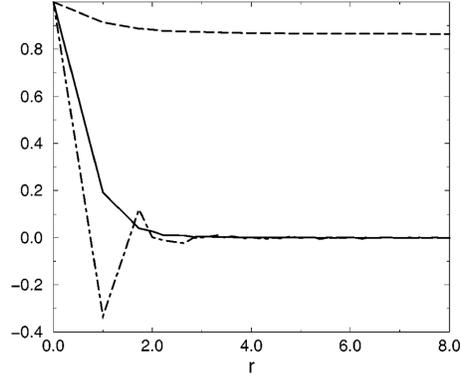
Figure 1.4: Correlation functions for the Heisenberg and XY antiferromagnets at a temperature of $5 \times 10^{-4}J$. The spin-spin correlation function is displayed with a dot-dashed line for a system of 2048 Heisenberg spins. This figure has been copied from [5].

Having seen the consequences of the frustration on classical spins on the pyrochlore lattice, we may ask how the extensive ground state degeneracy is reflected in the behavior of the quantum spins. For $S = 1$, the neutron scattering experiments on $\mathrm{NaCaNi_2F_7}$ suggest a spin liquid-like state at low temperatures [6] . For $S = \frac{1}{2}$, it is still an open question. Before discussing further, let us compare the ground states of S=1/2 spins in the triangle and the tetrahedron.

1.2 $S = 1/2$ spins on triangle and tetrahedron

1.2.1 Triangle

We saw, that the ground state of the triangle with classical spins is the state when the spins enclose $120°$. With quantum spins, it is completely different. The eight-dimensional Hilbert space of three $S = \frac{1}{2}$ spins, which are at the corners of the triangle, decomposes into two 2-dimensional $S = \frac{1}{2}$ (dublet) subspaces and a 4-dimensional $S = \frac{3}{2}$ (quadruplet) subspace:

$$\frac{1}{2} \otimes \frac{1}{2} \otimes \frac{1}{2} = \frac{1}{2} \oplus \frac{1}{2} \oplus \frac{3}{2} \ . \tag{1.7}$$

We get the ground state for antiferromagnetic case , when $S_{\mathrm{tot}} = \frac{1}{2}$ in the Eq. (1.3). It is satisfied, when two spins make a singlet bond, while the third remains free as on the Fig. (1.5). It is customary to denote the singlet bond between spins on site i and j as

$$[i, j] := \frac{1}{\sqrt{2}} |{\uparrow}{\downarrow} - {\downarrow}{\uparrow}\rangle. \tag{1.8}$$

Because of the minus sign, the singlet bonds are oriented, so $[i, j] = -[j, i]$. Using this notation we can write the states in Fig. 1.5 as $|[1, 2], {\uparrow}\rangle$, $|[2, 3], {\uparrow}\rangle$, and $|[3, 1], {\uparrow}\rangle$, from

left to right. Just two of these are linearly independent, since the sum of the three states cancels:

$$|[1,2],\uparrow\rangle + |[2,3],\uparrow\rangle + |[3,1],\uparrow\rangle = |\uparrow\downarrow\uparrow - \downarrow\uparrow\uparrow\rangle + |\uparrow\uparrow\downarrow - \uparrow\downarrow\uparrow\rangle + |\downarrow\uparrow\uparrow - \uparrow\uparrow\downarrow\rangle = 0. \quad (1.9)$$

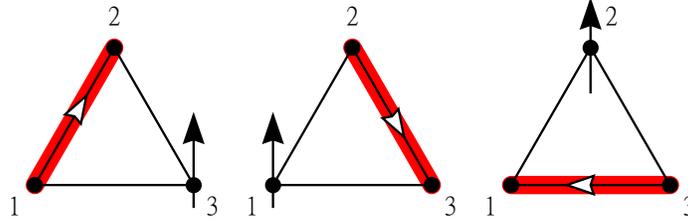Since the free spin can point up or down, the total degeneracy of the ground state is four.

Figure 1.5: Singlet bond configurations $|[1,2],\uparrow\rangle$, $|[2,3],\uparrow\rangle$, and $|[3,1],\uparrow\rangle$ (from left to right) on the triangle in the case of $S_{\text{tot}} = 1/2$.

The Heisenberg exchange can be rewritten with permutation operator:

$$P_{i,j} = 2\,\mathbf{S}_i \cdot \mathbf{S}_j + \frac{1}{2}\,, \quad (1.10)$$

where $P_{i,j}$ exchanges the spins on the sites i and j literally. For example, considering two sites only, $P_{1,2}|\uparrow\uparrow\rangle = |\uparrow\uparrow\rangle$ and $P_{1,2}|\uparrow\downarrow\rangle = |\downarrow\uparrow\rangle$. Furthermore, when it acts on a singlet bond $[i,j]$, we get $P_{i,j}[i,j] = [j,i] = -[i,j]$.

With the permutation operators, the Hamiltonian (1.2) for the triangle can be written as:

$$H = J \sum_{1 \leqslant i < j}^{3} \left(\frac{1}{2}P_{i,j} - \frac{1}{4} \right) = -\frac{3}{4}J + \frac{J}{2}(P_{1,2} + P_{1,3} + P_{2,3}) \quad (1.11)$$

The three permutation operators acting on the first configuration of Fig. (1.5):

$$(P_{1,2} + P_{1,3} + P_{2,3})\,|[1,2],\uparrow\rangle = |[2,1],\uparrow\rangle + |[3,2],\uparrow\rangle + |[1,3],\uparrow\rangle$$
$$= -\left(|[1,2],\uparrow\rangle + |[2,3],\uparrow\rangle + |[3,1],\uparrow\rangle \right). \quad (1.12)$$

As we have seen in Eq. (1.9), the last line in the equation above is equal to zero and we get

$$(P_{1,2} + P_{1,3} + P_{2,3})\,|[1,2],\uparrow\rangle = 0. \quad (1.13)$$

So taking the last equation into account, the first configuration of Fig. (1.5) is an eigenstate of the Heisenberg Hamiltonian with eigenvalue $-3J/4$,

$$H\,|[1,2],\uparrow\rangle = -\frac{3}{4}J\,|[1,2],\uparrow\rangle. \quad (1.14)$$

The remaining configurations in the $S_{\text{tot}} = 1/2$ subspace are also eigenstates, and ground states as well.

In the case, when $S_{\text{tot}} = 3/2$, $S_z = 3/2$ the

$$(P_{1,2} + P_{1,3} + P_{2,3}) \left| \uparrow\uparrow\uparrow \right\rangle = 3 \left| \uparrow\uparrow\uparrow \right\rangle, \tag{1.15}$$

so the eigenvalue is $\frac{3}{4}J$, and the same occurs for $S_z = -3/2$, or any other S_z state in the $S_{\text{tot}} = 3/2$ quartet. These results also follow from Eq. (3.1) in the special case of $N = 3$, which gives:

$$P_{1,2} + P_{1,3} + P_{2,3} = S_\triangle(S_\triangle + 1) - \frac{3}{4} = \begin{cases} 0, \ S_\triangle = 1/2 \\ 3, \ S_\triangle = 3/2 \end{cases}, \tag{1.16}$$

where $S_\triangle := S_{\text{tot}}$. Dividing the equation above by 3, we get

$$\mathcal{P}_\triangle = \frac{1}{3}(P_{1,2} + P_{1,3} + P_{2,3}) = \begin{cases} 0, \ S_\triangle = 1/2 \\ 1, \ S_\triangle = 3/2 \end{cases}, \tag{1.17}$$

which is a projector, with the property $\mathcal{P}_\triangle^2 = \mathcal{P}_\triangle$. We will use this projector to demonstrate the exact dimerized ground state for the Majumdar-Ghosh model.

1.2.2   Tetrahedron

Now we consider a tetrahedron, with four $S = \frac{1}{2}$ quantum spins at the corners. The 16-dimensional Hilbert space of the four $S = \frac{1}{2}$ spin decomposes into two 1-dimensional $S = 0$ (singlet), three 3-dimensional $S = 1$ (triplet), and one 5-dimensional $S = 2$ (quintuplet) subspace:

$$\frac{1}{2} \otimes \frac{1}{2} \otimes \frac{1}{2} \otimes \frac{1}{2} = 0 \oplus 0 \oplus 1 \oplus 1 \oplus 1 \oplus 2 . \tag{1.18}$$

The Hamiltonian can be written in the same form as Eq. (1.5). For antiferromagnetic exchange, this is minimal for $\mathbf{S}_{\text{tot}} = 0$, which is satisfied when the spins form singlet states. We need to pair the spins into two singlet bonds and this can be realized in three different ways, as illustrated in Fig. 1.6, and can be written as $\left| [1,2],[3,4] \right\rangle$, $\left| [1,3],[4,2] \right\rangle$ and $\left| [1,4],[2,3] \right\rangle$. Out of these configurations, only two states are linearly independent [7], in accordance with Eq. (1.18). We will show below that the sum of the three configurations is zero.
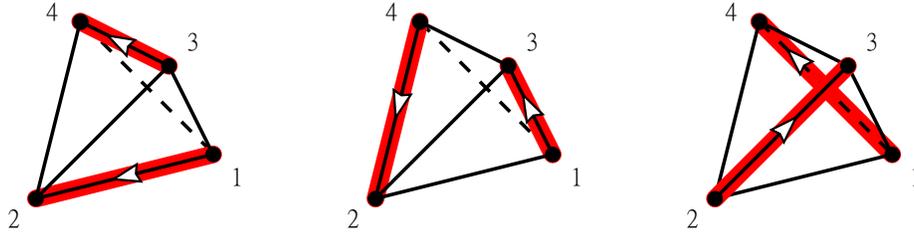
Figure 1.6: Singlet valence bond configurations (represented by thick red lines) $|[1,2],[3,4]\rangle$, $|[1,3],[4,2]\rangle$, and $|[1,4],[2,3]\rangle$ (from left to right) on the tetrahedron in the case of $S_{\mathrm{tot}} = 0$.

Let us separate these configurations as in the Fig. 1.7. and denote the states with the following convention: $|\uparrow_i\downarrow_j,[k,l]\rangle$, where $i < j$ and $i \neq j \neq k \neq l \in \{1,2,3,4\}$ and the indices denote the sites. In the following we leave the indices. With these, the states can be written as

$$|[1,2],[3,4]\rangle = |\uparrow\downarrow,[3,4]\rangle - |\downarrow\uparrow,[3,4]\rangle, \tag{1.19a}$$

$$|[1,3],[4,2]\rangle = |\uparrow\downarrow,[4,2]\rangle - |\downarrow\uparrow,[4,2]\rangle, \tag{1.19b}$$

$$|[1,4],[2,3]\rangle = |\uparrow\downarrow,[2,3]\rangle - |\downarrow\uparrow,[2,3]\rangle. \tag{1.19c}$$

Now consider just the states, when the site 1 has $|\uparrow\rangle$ spin: $|\uparrow\downarrow,[3,4]\rangle$, $|\uparrow\downarrow,[4,2]\rangle$ and $|\uparrow\downarrow,[2,3]\rangle$. In this case, the sum of the three states cancels (c.f. Eq. (1.7)):

$$|\uparrow\downarrow,[3,4]\rangle+|\uparrow\downarrow,[4,2]\rangle+|\uparrow\downarrow,[2,3]\rangle = |\uparrow\downarrow\uparrow\downarrow - \uparrow\downarrow\downarrow\uparrow\rangle+|\uparrow\downarrow\downarrow\uparrow - \uparrow\uparrow\downarrow\downarrow\rangle+|\uparrow\uparrow\downarrow\downarrow - \uparrow\downarrow\uparrow\downarrow\rangle = 0. \tag{1.20}$$

The same holds for the case when site 1 has $|\downarrow\rangle$ spin. Taking Eq. (1.19) into account, it follows that

$$|[1,2],[3,4]\rangle + |[1,3],[4,2]\rangle + |[1,4],[2,3]\rangle = 0, \tag{1.21}$$

so just two of the configurations are linearly independent, which was to be demonstrated.
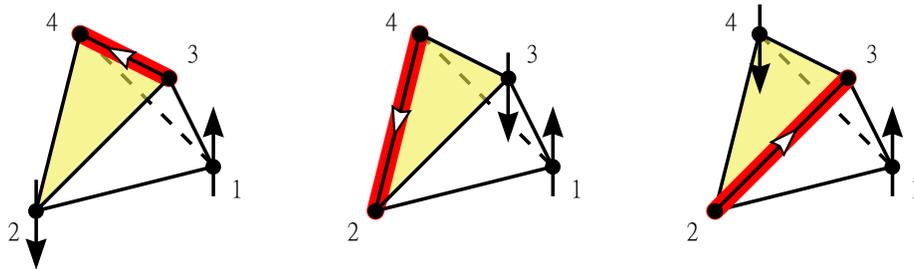

Figure 1.7: $S_{\mathrm{tot}} = 0$ configurations, where just 2 of the 4 spins forms singlet bonds (represented by thick red lines) and the remaining two $s = 1/2$ spins (black arrows).

As in the case of the triangle, the Hamiltonian (1.4) can be rewritten with permutations:

$$H = J \sum_{1 \leqslant i < j}^{4} \left(\frac{1}{2} P_{i,j} - \frac{1}{4} \right) = -J + P_{1,2} + P_{1,3} + P_{1,4} + P_{2,3} + P_{2,4} + P_{3,4} \qquad (1.22)$$

If we examine the effect of the sum of all permutations, it turns out, that it annihilates the singlets:

$$\begin{aligned}
&(P_{1,2} + P_{1,3} + P_{1,4} + P_{2,3} + P_{2,4} + P_{3,4}) \, |[1,2],[3,4]\rangle \\
&= -2 \left(|[1,2],[3,4]\rangle + |[2,3],[1,4]\rangle + |[4,2],[1,3]\rangle \right) \\
&= 0, \qquad\qquad\qquad\qquad\qquad\qquad\qquad\qquad\qquad\qquad\qquad\qquad (1.23)
\end{aligned}$$

just like in the case of the triangle Eq. (1.13). The singlets are eigenstates of the Hamiltonian and also ground state with eigenvalue $-J$.

When $S_{\text{tet}} = 1$ or $S_{\text{tet}} = 2$, where $S_{\text{tet}} := S_{\text{tot}}$, we can get the effect of the sum of all permutation from the special case ($N = 4$) of the Eq. (3.1):

$$P_{1,2} + P_{1,3} + P_{1,4} + P_{2,3} + P_{2,4} + P_{3,4} = S_{\text{tet}}(S_{\text{tet}} + 1) = \begin{cases} 0, & S_{\text{tet}} = 0 \\ 2, & S_{\text{tet}} = 1 \\ 6, & S_{\text{tet}} = 2 \end{cases} . \qquad (1.24)$$

It is clear from Eq. (1.24) that we can't construct a projection only with the $P_{i,j}$ 2 site exchanges, we need to apply other terms. Let us introduce the notation

$$P_{\text{tet}}^{(2)} = P_{1,2} + P_{1,3} + P_{1,4} + P_{2,3} + P_{2,4} + P_{3,4}, \qquad (1.25)$$

$$P_{\text{tet}}^{(4)} = P_{1,2}P_{3,4} + P_{1,3}P_{2,4} + P_{1,4}P_{2,3}. \qquad (1.26)$$

The $P_{\text{tet}}^{(2)}$ is the sum of the usual exchanges on the bonds of the tetrahedron, and the origin of the $P_{\text{tet}}^{(4)}$ is the four-spin ring exchange. $P_{\text{tet}}^{(4)}$ is useful to express the square of $P_{\text{tet}}^{(2)}$, since

$$(P_{\text{tet}}^{(2)})^2 = -6P_0 + 6P_{\text{tet}}^{(2)} + 2P_{\text{tet}}^{(4)}, \qquad (1.27)$$

where P_0 is the identity permutation. There is no further term appearing for a fully symmetric tetrahedron with the T_d symmetry. The eigenvalues of the Hamiltonian including also the four spin terms,

$$H_{\text{tet}} = a_0 P_0 + a_2 P_{\text{tet}}^{(2)} + a_4 P_{\text{tet}}^{(4)} \qquad (1.28)$$

are

$$E(S_{\text{tet}} = 0) = a_0 + 3a_4 \qquad (1.29)$$

$$E(S_{\text{tet}} = 1) = a_0 + 2a_2 - a_4 \qquad (1.30)$$

$$E(S_{\text{tet}} = 2) = a_0 + 6a_2 + 3a_4 \qquad (1.31)$$

From this we can construct the projector $\mathcal{P}_{\text{tet}}$ which annihilates the singlets and projects out the $S_{\text{tet}} = 1$ and $S_{\text{tet}} = 2$ states.

$$\mathcal{P}_{\text{tet}} = \frac{1}{2}P_0 + \frac{1}{6}P_{\text{tet}}^{(2)} - \frac{1}{6}P_{\text{tet}}^{(4)}. \tag{1.32}$$

It satisfies the $(\mathcal{P}_{\text{tet}})^2 = \mathcal{P}_{\text{tet}}$ property of a projector, so that the eigenvalues are either zeroes and ones.

1.3 Majumdar-Ghosh Hamitonian for the $S = 1/2$ spin chain

The one-dimensional $S = \frac{1}{2}$ Heisenberg chain, with nearest neighbor (J_1) interaction, is exactly solvable by Bethe Ansatz, with a gapless spectrum [8]. If we add the next-nearest neighbor interaction J_2, around $J_2/J_1 \approx 0.24$ a quantum phase transition into a gapped, dimerized phase occurs [9]. The Heisenberg chain Hamiltonian with J_1 and J_2 interaction on N sites reads

$$H = \sum_{i=1}^{N} J_1 \mathbf{S}_i \cdot \mathbf{S}_{i+1} + J_2 \mathbf{S}_i \cdot \mathbf{S}_{i+2} , \tag{1.33}$$

where $\mathbf{S}_{N+1} = \mathbf{S}_1$ and $\mathbf{S}_{N+2} = \mathbf{S}_2$ when a periodic boundary condition is assumed.
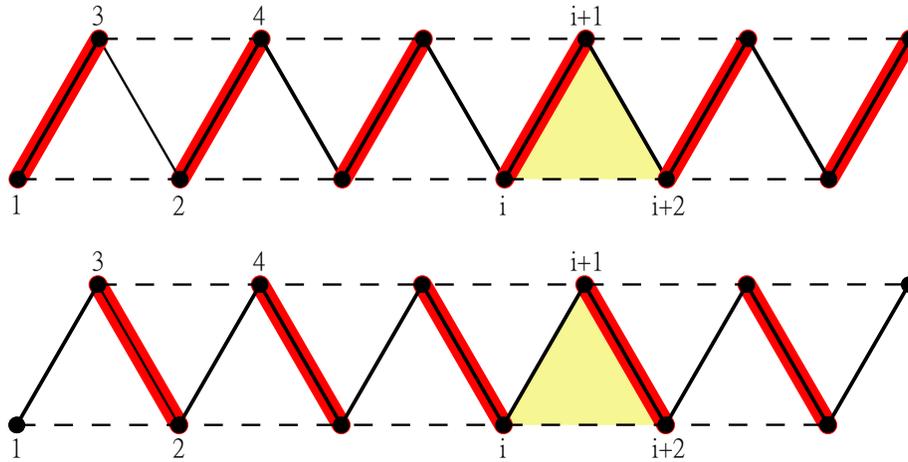
Figure 1.8: The dimerized ground states of the Majumdar-Ghosh Hamiltonian. Dashed lines denote the next nearest neighbor exchange J_2 and the solid lines stand for J_1. The ground states, $[1,2][3,4]\ldots$ and $[N,1][2,3][4,5]\ldots$, are products of the singlet valence bonds (represented by thick red lines) and break translational invariance.

When we add the J_2 next neighbor exchange, the model is not solvable analytically by Bethe Ansatz anymore. However, at a special point $J_2/J_1 = \frac{1}{2}$ (Majumdar-Ghosh point),

the ground state can be expressed by the product of spin singlet bonds shown in Fig. 1.8. Below we will show that this is an exact eigenstate of the model. The Hamiltonian (1.33) at the Majumdar-Ghosh point becomes

$$H_{\text{MG}} = J \sum_{i=1}^{N} \left(\mathbf{S}_i \cdot \mathbf{S}_{i+1} + \frac{1}{2} \mathbf{S}_i \cdot \mathbf{S}_{i+2} \right) . \tag{1.34}$$

This can be rewritten as a sum of full squares:

$$H_{\text{MG}} = -\frac{3}{4} JN + \frac{1}{4} J \sum_{i=1}^{N} \left(\mathbf{S}_i + \mathbf{S}_{i+1} + \mathbf{S}_{i+2} \right)^2 . \tag{1.35}$$

The total spin at sites $(i, i+1, i+2)$ is $\mathbf{S}_i^{\text{tot}} = \mathbf{S}_i + \mathbf{S}_{i+1} + \mathbf{S}_{i+2}$ (the yellow triangle in Fig. 1.8). Its square has eigenvalues $S_i^{\text{tot}}(S_i^{\text{tot}} + 1)$, where $S_i^{\text{tot}} = \frac{1}{2}, \frac{3}{2}$. From this we can easily construct a projection:

$$\mathcal{P}_i^{\text{MG}} = \frac{1}{3} (\mathbf{S}_i^{\text{tot}})^2 - \frac{1}{4} , \tag{1.36}$$

which gives 0 for $S_i^{\text{tot}} = \frac{1}{2}$ and 1 for $S_i^{\text{tot}} = \frac{3}{2}$. In the Sec. 1.2.1 we have already encountered this problem for a single triangle, where we expressed the Hamiltonian (1.2) of the triangle using a projection operator. Following Eq. (1.17), we may define the projection operator acting on three consecutive sites as

$$\mathcal{P}_i^{\text{MG}} = \frac{1}{3} (P_{i,i+1} + P_{i,i+2} + P_{i+1,i+2}) = \begin{cases} 0, & \text{for } S_i^{\text{tot}} = 1/2 \\ 1, & \text{for } S_i^{\text{tot}} = 3/2 \end{cases} . \tag{1.37}$$

With this, the Hamiltonian can be rewritten as:

$$H_{\text{MG}} = -\frac{3}{8} JN + \frac{3}{4} J \sum_{i=1}^{N} \mathcal{P}_i^{\text{MG}} . \tag{1.38}$$

Since the Hamiltonian is the sum of projectors with positive coefficients when $J > 0$, it is clear that the Hamiltonian is minimal when all the projectors $\mathcal{P}_i^{\text{MG}}$ give 0 eigenvalue. This can also be seen from Eq. (1.13), since the wave functions $[1,2][3,4]\ldots$ and $[N,1][2,3][4,5]\ldots$, depicted in Fig. 1.8, contain a singlet bond in each triangle consisting of three consecutive sites $i, i+1$, and $i+2$. Therefore we have shown that the ground state is two-fold degenerate and breaks the translational symmetry.

Chapter 2

The spin-1/2 Heisenberg model on the pyrochlore lattice

We briefly covered the classical spins in the pyrochlore lattice in the introduction. The behavior of the classical spins is well understood – the spins remain disordered, but they obey the tetrahedron rule, Eq. (1.6). On the other hand, the behavior of the $S = 1/2$ spin is still debated. We lack exact analytical results, and the numerical treatment of this three–dimensional interacting model is difficult. Recent results include the application of the density matrix renormalization group method to system up to 128 sites, where an inversion symmetry breaking ground state has been found [1]. On the other hand, the pseudofermion functional renormalization group method found an extended quantum-spin-liquid phase robust against the introduction of breathing anisotropy [10]. These are cutting edge numerical methods, and the controversy shows the difficulty of the problem.

Our aim is to construct a $S = 1/2$ Hamiltonian which has the tetramerized states as exact ground states, just like the Majumdar-Ghosh Hamiltonian has the dimerized states as exact ground states. We will first approach this problem by constructing a projector,

2.1   The projector approach

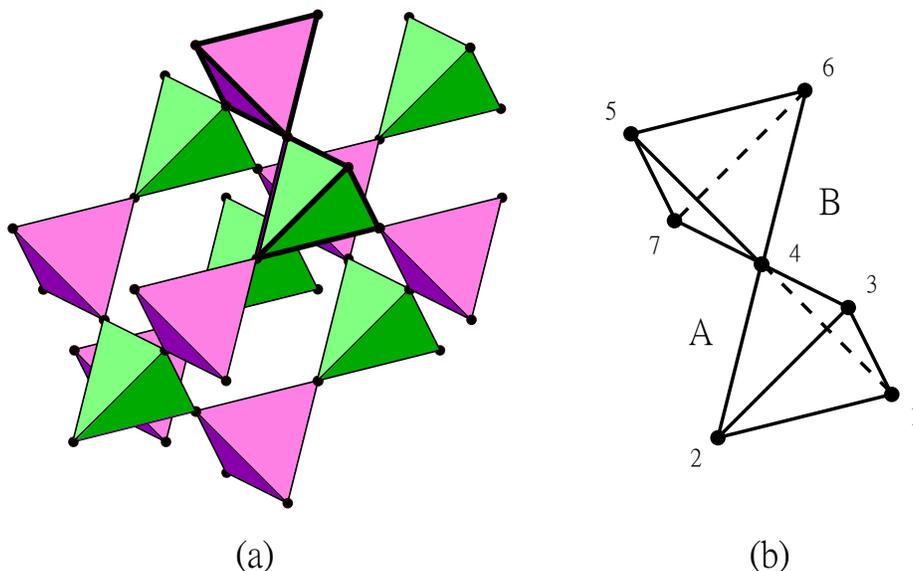(a)   (b)

Figure 2.1: The pyrochlore lattice in the (a), and the motif in the (b) figure, where A denotes the Green and B the Magenta color.

We require from our model to spontaneously break the inversion symmetry, which is achieved, when either the green (A) or the magenta tetrahedra (B) of the pyrochlore lattice, shown in Fig. 2.1(a), form a spin-singlet state. Denoting by $|0_A\rangle$ a spin singlet configuration on an A-type tetrahedron, the wave function is the product of the singlets over all the A tetrahedra,

$$|\psi_A\rangle = \prod_{\text{A tetrahedra}} |0_A\rangle \ . \tag{2.1}$$

This is for example the wave function of the so-called breathing pyrochlore [11], where only the exchanges on the bonds of the green (A) tetrahedra are finite, on the bonds belonging to the magenta (B) tetrahedra are vanishingly small – this is the limit of decoupled tetrahedra. In Sec. 1.2.2 we considered the eigenstates of the Heisenberg model on a single tetrahedron. We found out that the singlet ground state is two-fold degenerate. The $|0_A\rangle$ in the $|\psi_A\rangle$ denotes any of those two singlets, and which we allow to be in different linear combinations on different tetrahedra. Taking all possible configurations, the $|\psi_A\rangle$ wave functions will span a linear space of dimension $2^{N_A} = 2^{N_{\text{tet}}/2}$, where $N_A = N_{\text{tet}}/2$ is the number of A tetrahedra – we will call this linear space as the $\mathcal{M}_A$ ground state manifold. In other words, the $\mathcal{M}_A$ is the direct product of the two-dimensional singlet manifolds of the A tetrahedra,

$$\mathcal{M}_A = \{|0_{A_1}\rangle_1, |0_{A_1}\rangle_2\} \otimes \{|0_{A_2}\rangle_1, |0_{A_2}\rangle_2\} \otimes \cdots \otimes \left\{\left|0_{A_{N_A}}\right\rangle_1, \left|0_{A_{N_A}}\right\rangle_2\right\} \ . \tag{2.2}$$

We can similarly construct the states with singlets on the B tetrahedra,

$$|\psi_\mathrm{B}\rangle = \prod_{\mathcal{M}_\mathrm{B}} |0_\mathrm{B}\rangle \ . \tag{2.3}$$

These states will make the $\mathcal{M}_\mathrm{B}$ manifold.

We aim to construct a Hamiltonian $\mathcal{H}$ for which the states above will be ground states with 0 eigenvalues:

$$\mathcal{H}|\psi\rangle = 0, \quad \text{when } |\psi\rangle \in \mathcal{M}_{\mathrm{A}\cup\mathrm{B}} \ . \tag{2.4}$$

Following the idea of the Majumdar-Ghosh model, we will write the Hamiltonian $\mathcal{H}$ as the sum of projectors $\mathcal{P}$

$$\mathcal{H} = \sum_{g \in G} g\mathcal{P}. \tag{2.5}$$

Here $\mathcal{P}$ means a single operator that has been translated and rotated by the elements g of the space group G.

For all $|\psi_\mathrm{A}\rangle$ and $|\psi_\mathrm{B}\rangle \in \mathcal{M}_{\mathrm{A}\cup\mathrm{B}}$, the $g\mathcal{P}|\psi_\mathrm{A}\rangle$ and $g\mathcal{P}|\psi_\mathrm{B}\rangle$ should give zero,

$$g\mathcal{P}|\psi_\mathrm{A}\rangle = 0 \ , \tag{2.6a}$$
$$g\mathcal{P}|\psi_\mathrm{B}\rangle = 0 \ , \tag{2.6b}$$

for any $g \in G$. In the following, we will identify an operator $\mathcal{P}$ which extends over 7 sites. These 7 sites form a motif consisting of two corner-sharing tetrahedra (a magenta and a green one), shown in Fig. 2.1. The motif is large enough to contain the singlet on either of the tetrahedra (A or B). We will assume the notation of the sites as given in Fig. 2.1(b).
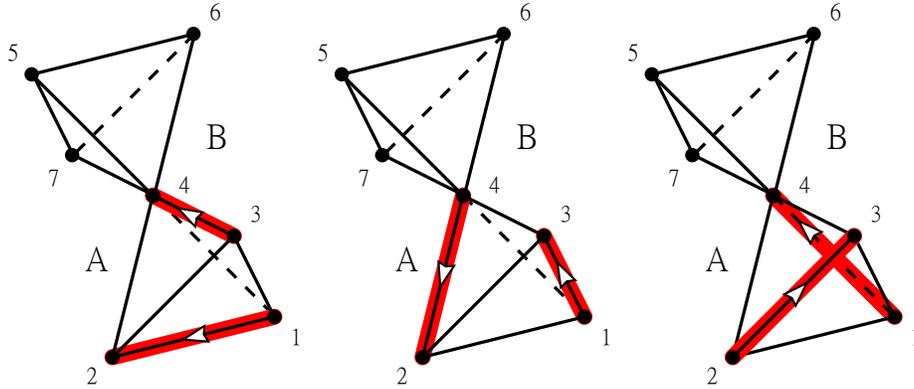

Figure 2.2: Possible ground states of the motif, where the spins form singlet bonds on the A tetrahedron.

To construct the projector of the motif, consider the state-A case, which can be seen in Fig. 2.2. When we restrict the wave functions in $\mathcal{M}_\mathrm{A}$ to the seven sites of the motif, the

singlet being at A tetrahedron means that the singlet is formed at sites 1,2,3, and 4, and the projector shall have 0 eigenvalues with the following wave functions:

$$[1,2][3,4]\sigma_5\sigma_6\sigma_7 \; , \tag{2.7a}$$

$$[1,3][4,2]\sigma_5\sigma_6\sigma_7 \; , \tag{2.7b}$$

$$[1,4][2,3]\sigma_5\sigma_6\sigma_7 \; , \tag{2.7c}$$

depicted in Fig. 2.2 from left to right. The valence bonds $[1,2][3,4]$ in Eq. (2.7a) ensure that spins at sites 1,2,3, and 4 form a singlet, and the remaining spins at sites 5,6, and 7 are arbitrary (they take part in another singlet which is outside of the motif). Naively, the ground state would be $3 \cdot 2^3 = 24$ degenerate, but from the three singlet configurations just two are linearly independent (see Sec. 1.2.2). Then, the dimension of the ground-state manifold restricted to the motif, $\mathcal{M}_{\mathrm{A}}^{\mathrm{motif}}$, is $2 \cdot 2^3 = 16$. Similarly, we can consider the case when the singlet is at the B (magenta) tetrahedron. The spins at sites 4,5,6, and 7 will make a singlet, and they will increase the dimension of the ground-state manifold, now $\mathcal{M}_{\mathrm{A}\cup\mathrm{B}}^{\mathrm{motif}}$, to $2 \times 16 = 32$.

It would be a difficult task to determine these manifolds by hand. Therefore we will use `Mathematica` to perform these calculations. First, we constructed basis vectors in the $2^7 = 128$ dimensional Hilbert space. Next, we constructed the 8 configurations of Eq. (2.7a) as the ground state manifold of the Hamiltonian $P_{1,2} + P_{3,4}$, following the construction of the matrix representations of the permutations in the 128 dimensional Hilbert space and numerically diagonalizing it. We repeated the procedure to construct configurations of Eq. (2.7b) by taking the ground state manifold of the Hamiltonian $P_{1,3} + P_{2,4}$, and so on. To get the $\mathcal{M}_{\mathrm{A}}^{\mathrm{motif}}$, we collected the linearly independent eigenvectors. Repeating these for the case of when the singlet is on the B tetrahedron, we get the manifold $\mathcal{M}_{\mathrm{B}}^{\mathrm{motif}}$. Then the manifold of the projection is the collection of the linearly independent eigenvectors of $\mathcal{M}_{\mathrm{A}}^{\mathrm{motif}}$ and $\mathcal{M}_{\mathrm{B}}^{\mathrm{motif}}$,

$$\mathcal{M}_{\mathrm{A}\cup\mathrm{B}}^{\mathrm{motif}} = \mathcal{M}_{\mathrm{A}}^{\mathrm{motif}} \bigcup \mathcal{M}_{\mathrm{B}}^{\mathrm{motif}}. \tag{2.8}$$

Then the projection $\mathcal{P}$ we search for is just

$$\mathcal{P} = 1 - \sum_{|\alpha\rangle\in\mathcal{M}_{\mathrm{A}\cup\mathrm{B}}^{\mathrm{motif}}} |\alpha\rangle\langle\alpha| \; . \tag{2.9}$$

To get the projection in the form of permutations, we collect all the permutation (P_i) over the index set $\{1, 2, 3, ..., 7\}$, whose order $|P_i| \leqslant 2$. Denote this set P. Then taking $P_i \in P$, with coefficient c_i, we can get the projector with permutations:

$$\mathcal{P} = \sum_{P_i\in P} c_i M_{P_i} \; , \tag{2.10}$$

where M_{P_i} is the matrix representation of P_i in the 128 dimensional Hilbert-space. Comparing Eq. (2.9) with the equation above, we can determine each c_i and P_i. We have collected the different terms in Tab. 2.1.

Coefficient	Permutations
$-1/6$	$P_{1,2}$, $P_{1,3}$, $P_{2,3}$, $P_{5,6}$, $P_{5,7}$, $P_{6,7}$
$-1/9$	$P_{1,4}$, $P_{2,4}$, $P_{3,4}$, $P_{4,5}$, $P_{4,6}$, $P_{4,7}$
$-1/27$	$P_{1,5}$, $P_{1,6}$, $P_{1,7}$, $P_{2,5}$, $P_{2,6}$, $P_{2,7}$, $P_{3,5}$, $P_{3,6}$, $P_{3,7}$, $P_{1,2}P_{3,5}P_{6,7}$, $P_{1,2}P_{3,6}P_{5,7}$, $P_{1,2}P_{3,7}P_{5,6}$, $P_{1,3}P_{2,5}P_{6,7}$, $P_{1,3}P_{2,6}P_{5,7}$, $P_{1,3}P_{2,7}P_{5,6}$, $P_{1,5}P_{2,3}P_{6,7}$, $P_{1,6}P_{2,3}P_{5,7}$, $P_{1,7}P_{2,3}P_{5,6}$
$-1/54$	$P_{1,2}P_{4,5}$, $P_{1,2}P_{4,6}$, $P_{1,2}P_{4,7}$, $P_{1,3}P_{4,5}$, $P_{1,3}P_{4,6}$, $P_{1,3}P_{4,7}$, $P_{1,4}P_{5,6}$, $P_{1,4}P_{5,7}$, $P_{1,4}P_{6,7}$, $P_{2,3}P_{4,5}$, $P_{2,3}P_{4,6}$, $P_{2,3}P_{4,7}$, $P_{2,4}P_{5,6}$, $P_{2,4}P_{5,7}$, $P_{2,4}P_{6,7}$, $P_{3,4}P_{5,6}$, $P_{3,4}P_{5,7}$, $P_{3,4}P_{6,7}$
$1/54$	$P_{1,2}P_{3,4}P_{5,6}$, $P_{1,2}P_{3,4}P_{5,7}$, $P_{1,2}P_{3,4}P_{6,7}$, $P_{1,2}P_{4,5}P_{6,7}$, $P_{1,2}P_{4,6}P_{5,7}$, $P_{1,2}P_{4,7}P_{5,6}$, $P_{1,3}P_{2,4}P_{5,6}$, $P_{1,3}P_{2,4}P_{5,7}$, $P_{1,3}P_{2,4}P_{6,7}$, $P_{1,3}P_{4,5}P_{6,7}$, $P_{1,3}P_{4,6}P_{5,7}$, $P_{1,3}P_{4,7}P_{5,6}$, $P_{1,4}P_{2,3}P_{5,6}$, $P_{1,4}P_{2,3}P_{5,7}$, $P_{1,4}P_{2,3}P_{6,7}$, $P_{2,3}P_{4,5}P_{6,7}$, $P_{2,3}P_{4,6}P_{5,7}$, $P_{2,3}P_{4,7}P_{5,6}$
$1/27$	$P_{1,2}P_{3,5}$, $P_{1,2}P_{3,6}$, $P_{1,2}P_{3,7}$, $P_{1,3}P_{2,5}$, $P_{1,3}P_{2,6}$, $P_{1,3}P_{2,7}$, $P_{1,5}P_{2,3}$, $P_{1,5}P_{6,7}$, $P_{1,6}P_{2,3}$, $P_{1,6}P_{5,7}$, $P_{1,7}P_{2,3}$, $P_{1,7}P_{5,6}$, $P_{2,5}P_{6,7}$, $P_{2,6}P_{5,7}$, $P_{2,7}P_{5,6}$, $P_{3,5}P_{6,7}$, $P_{3,6}P_{5,7}$, $P_{3,7}P_{5,6}$
$1/9$	$P_{1,2}P_{3,4}$, $P_{1,3}P_{2,4}$, $P_{1,4}P_{2,3}$, $P_{4,5}P_{6,7}$, $P_{4,6}P_{5,7}$, $P_{4,7}P_{5,6}$
1	P_0

Table 2.1: The permutations (second column) and their coefficient (first column) in Eq. (2.10) of the projector. In the last row, the P_0 denotes the identity permutation.

Altogether, we determined a Hamiltonian whose ground states spontaneously break inversion symmetry. The Hamiltonian is the sum of projectors $\mathcal{P}$ which satisfy the $\mathcal{P}^2 = \mathcal{P}$ property of projection and the singlet product wave functions are ground states with zero eigenvalue: $\mathcal{P} |\psi_A\rangle = 0$ and $\mathcal{P} |\psi_B\rangle = 0$. The projector is cumbersome (for example it contains 6-site exchanges) and it is difficult to interpret its physical meaning. The reason for this complicated form is that the remaining $128 - 32 = 96$ states all need to have eigenvalue 1. Starting from this observation, in the next sections, we are trying to find simpler and meaningful Hamiltonians with the same ground state manifold.

2.2 The Hamiltonian

In this section, we are trying to find an appropriate Hamiltonian $\mathcal{H}_{\mathrm{motif}}$, which can replace the projector $\mathcal{P}$ we created in the previous section. For a starting point, we require for $\mathcal{H}_{\mathrm{motif}}$ to respect the D_{3d} point group symmetry of the motif. The generators of D_{3d} group can be expressed using the site permutations as

$$i = P_{1,5}P_{2,6}P_{3,7} \tag{2.11a}$$

$$C_3 = P_{1,2,3}P_{5,6,7} \tag{2.11b}$$

$$\sigma_d = P_{2,3}P_{6,7} \,, \tag{2.11c}$$

where i is the inversion, C_3 is the rotation by $2\pi/3$ and σ_d is a reflection. We follow the site numbering of Fig. 2.1(b). To construct a Hamiltonian, we take all the permutations of the motif, which contain 2- and 4-site exchanges. In the language of permutations, the set of all 2-site $P_{i,j}$, where $i \neq j \in \{1, 2, 3, ..., 7\}$, the set of all 4-site $P_{i,j}P_{k,l}$, where the sites $i, j, k, l \in \{1, 2, 3, ..., 7\}$ are all different, and the identity permutation P_0. Acting on each

permutation with the elements of the group, we get 19 orbits of the permutations. The permutations in the same orbit will have the same weights in the Hamiltonian. The sum of the permutations with their weights in matrix representation in the 128 dimensional Hilbert-space, will provide us a $\mathcal{H}_{\mathrm{motif}}$ with 19 parameter $h_1, h_2, ..., h_{19}$. The orbits are collected in Tab. 2.2.

Parameter	Permutations
h_1	P_0
h_2	$P_{1,5}, \ P_{2,6}, \ P_{3,7}$
h_3	$P_{1,2}, \ P_{1,3}, \ P_{2,3}, \ P_{5,6}, \ P_{5,7}, \ P_{6,7}$
h_4	$P_{1,4}, \ P_{2,4}, \ P_{3,4}, \ P_{4,5}, \ P_{4,6}, \ P_{4,7}$
h_5	$P_{1,6}, \ P_{1,7}, \ P_{2,5}, \ P_{2,7}, \ P_{3,5}, \ P_{3,6}$
h_6	$P_{1,2}P_{5,6}, \ P_{1,3}P_{5,7}, \ P_{2,3}P_{6,7}$
h_7	$P_{1,5}P_{2,6}, \ P_{1,5}P_{3,7}, \ P_{2,6}P_{3,7}$
h_8	$P_{1,6}P_{2,5}, \ P_{1,7}P_{3,5}, \ P_{2,7}P_{3,6}$
h_9	$P_{1,2}P_{3,4}, \ P_{1,3}P_{2,4}, \ P_{1,4}P_{2,3}, \ P_{4,5}P_{6,7}, \ P_{4,6}P_{5,7}, \ P_{4,7}P_{5,6}$
h_{10}	$P_{1,2}P_{3,7}, \ P_{1,3}P_{2,6}, \ P_{1,5}P_{2,3}, \ P_{1,5}P_{6,7}, \ P_{2,6}P_{5,7}, \ P_{3,7}P_{5,6}$
h_{11}	$P_{1,2}P_{4,7}, \ P_{1,3}P_{4,6}, \ P_{1,4}P_{6,7}, \ P_{2,3}P_{4,5}, \ P_{2,4}P_{5,7}, \ P_{3,4}P_{5,6}$
h_{12}	$P_{1,2}P_{5,7}, \ P_{1,2}P_{6,7}, \ P_{1,3}P_{5,6}, \ P_{1,3}P_{6,7}, \ P_{2,3}P_{5,6}, \ P_{2,3}P_{5,7}$
h_{13}	$P_{1,5}P_{2,7}, \ P_{1,5}P_{3,6}, \ P_{1,6}P_{3,7}, \ P_{1,7}P_{2,6}, \ P_{2,5}P_{3,7}, \ P_{2,6}P_{3,5}$
h_{14}	$P_{1,6}P_{2,7}, \ P_{1,6}P_{3,5}, \ P_{1,7}P_{2,5}, \ P_{1,7}P_{3,6}, \ P_{2,5}P_{3,6}, \ P_{2,7}P_{3,5}$
h_{15}	$P_{1,2}P_{3,5}, \ P_{1,2}P_{3,6}, \ P_{1,3}P_{2,5}, \ P_{1,3}P_{2,7}, \ P_{1,6}P_{2,3}, \ P_{1,6}P_{5,7},$ $P_{1,7}P_{2,3}, \ P_{1,7}P_{5,6}, \ P_{2,5}P_{6,7}, \ P_{2,7}P_{5,6}, \ P_{3,5}P_{6,7}, \ P_{3,6}P_{5,7}$
h_{16}	$P_{1,2}P_{4,5}, \ P_{1,2}P_{4,6}, \ P_{1,3}P_{4,5}, \ P_{1,3}P_{4,7}, \ P_{1,4}P_{5,6}, \ P_{1,4}P_{5,7},$ $P_{2,3}P_{4,6}, \ P_{2,3}P_{4,7}, \ P_{2,4}P_{5,6}, \ P_{2,4}P_{6,7}, \ P_{3,4}P_{5,7}, \ P_{3,4}P_{6,7}$
h_{17}	$P_{1,4}P_{2,5}, \ P_{1,4}P_{3,5}, \ P_{1,6}P_{2,4}, \ P_{1,6}P_{4,5}, \ P_{1,7}P_{3,4}, \ P_{1,7}P_{4,5},$ $P_{2,4}P_{3,6}, \ P_{2,5}P_{4,6}, \ P_{2,7}P_{3,4}, \ P_{2,7}P_{4,6}, \ P_{3,5}P_{4,7}, \ P_{3,6}P_{4,7}$
h_{18}	$P_{1,4}P_{2,6}, \ P_{1,4}P_{3,7}, \ P_{1,5}P_{2,4}, \ P_{1,5}P_{3,4}, \ P_{1,5}P_{4,6}, \ P_{1,5}P_{4,7},$ $P_{2,4}P_{3,7}, \ P_{2,6}P_{3,4}, \ P_{2,6}P_{4,5}, \ P_{2,6}P_{4,7}, \ P_{3,7}P_{4,5}, \ P_{3,7}P_{4,6}$
h_{19}	$P_{1,4}P_{2,7}, \ P_{1,4}P_{3,6}, \ P_{1,6}P_{3,4}, \ P_{1,6}P_{4,7}, \ P_{1,7}P_{2,4}, \ P_{1,7}P_{4,6},$ $P_{2,4}P_{3,5}, \ P_{2,5}P_{3,4}, \ P_{2,5}P_{4,7}, \ P_{2,7}P_{4,5}, \ P_{3,5}P_{4,6}, \ P_{3,6}P_{4,5}$

Table 2.2: Different orbits of the permutation (second column) and their weights (first column).

To have the same eigenstates as the projector, we require for the Hamiltonian to commute with the projection operator $\mathcal{P}$:

$$\left[\mathcal{H}_{\mathrm{motif}}, \mathcal{P}\right] = 0. \tag{2.12}$$

This condition reduces the number of the independent parameters from 19 to 12, which are listed in the first column in Tab. (2.3). Moreover, the Hamiltonian should satisfy for all

$|\psi\rangle \in \mathcal{M}_{\mathrm{A\cup B}}^{\mathrm{motif}}$ the

$$\mathcal{H}_{\mathrm{motif}} |\psi\rangle = 0 \tag{2.13}$$

equation. This left us 7 independent parameters $g_1, g_2, ..., g_7$, which are displayed in the second column in Tab. 2.3.

To recapitulate, we get a 7-parameter Hamiltonian for which the states in the $\mathcal{M}_{\mathrm{A\cup B}}$ are exact eigenstate with 0 eigenvalue. However, they are not necessarily ground states, as the spectrum can have other states with lower energy. We need to find such a combination of g_i's which will ensure that all the other states have positive energies. For this, we need to determine the eigenvalues of the Hamiltonian.

Parameters satisfying $[\mathcal{H}_{\mathrm{motif}}, \mathcal{P}] = 0$	Parameters satisfying $\mathcal{H}_{\mathrm{motif}} |\psi\rangle = 0$	Permutations
h_1	$15g_1$	P_0
h_2	$10g_2$	$P_{1,5}, \; P_{2,6}, \; P_{3,7}$
h_3	$5g_3$	$P_{1,2}, \; P_{1,3}, \; P_{2,3}, \; P_{5,6}, \; P_{5,7}, \; P_{6,7}$
h_4	$10g_4$	$P_{1,4}, \; P_{2,4}, \; P_{3,4}, \; P_{4,5}, \; P_{4,6}, \; P_{4,7}$
h_5	$5g_5$	$P_{1,6}, \; P_{1,7}, \; P_{2,5}, \; P_{2,7}, \; P_{3,5}, \; P_{3,6}$
h_6	g_6	$P_{1,2}P_{5,6}, \; P_{1,3}P_{5,7}, \; P_{2,3}P_{6,7}$
h_7	$-g_1 + 4g_2 - 2g_3 + 4g_4 - 6g_5$	$P_{1,5}P_{2,6}, \; P_{1,5}P_{3,7}, \; P_{2,6}P_{3,7}$
h_8	$-g_1 + 4g_2 - 2g_3 + 4g_4 - 6g_5$	$P_{1,6}P_{2,5}, \; P_{1,7}P_{3,5}, \; P_{2,7}P_{3,6}$
h_9	$-g_1 - g_2 - 2g_3 - g_4 - g_5$	$P_{1,2}P_{3,4}, \; P_{1,3}P_{2,4}, \; P_{1,4}P_{2,3}, \; P_{4,5}P_{6,7}, \; P_{4,6}P_{5,7}, \; P_{4,7}P_{5,6}$
$-h_2 - h_4 + 2h_5 + h_7 + h_8 - h_9$	$-g_1 - g_2 - 2g_3 - g_4 - g_5$	$P_{1,2}P_{3,7}, \; P_{1,3}P_{2,6}, \; P_{1,5}P_{2,3}, \; P_{1,5}P_{6,7}, \; P_{2,6}P_{5,7}, \; P_{3,7}P_{5,6}$
h_{11}	g_7	$P_{1,2}P_{4,7}, \; P_{1,3}P_{4,6}, \; P_{1,4}P_{6,7}, \; P_{2,3}P_{4,5}, \; P_{2,4}P_{5,7}, \; P_{3,4}P_{5,6}$
h_{12}	$-10g_2 + 5g_5 + g_6$	$P_{1,2}P_{5,7}, \; P_{1,2}P_{6,7}, \; P_{1,3}P_{5,6}, \; P_{1,3}P_{6,7}, \; P_{2,3}P_{5,6}, \; P_{2,3}P_{5,7}$
$-h_2 + h_5 + h_8$	$-g_1 - 6g_2 - 2g_3 + 4g_4 - g_5$	$P_{1,5}P_{2,7}, \; P_{1,5}P_{3,6}, \; P_{1,6}P_{3,7}, \; P_{1,7}P_{2,6}, \; P_{2,5}P_{3,7}, \; P_{2,6}P_{3,5}$
$-h_2 + h_5 + h_7$	$-g_1 - 6g_2 - 2g_3 + 4g_4 - g_5$	$P_{1,6}P_{2,7}, \; P_{1,6}P_{3,5}, \; P_{1,7}P_{2,5}, \; P_{1,7}P_{3,6}, \; P_{2,5}P_{3,6}, \; P_{2,7}P_{3,5}$
$-h_2 - h_4 + 2h_5 + h_7 + h_8 - h_9$	$-g_1 - g_2 - 2g_3 - g_4 - g_5$	$P_{1,2}P_{3,5}, \; P_{1,2}P_{3,6}, \; P_{1,3}P_{2,5}, \; P_{1,3}P_{2,7}, \; P_{1,6}P_{2,3}, \; P_{1,6}P_{5,7},$ $P_{1,7}P_{2,3}, \; P_{1,7}P_{5,6}, \; P_{2,5}P_{6,7}, \; P_{2,7}P_{5,6}, \; P_{3,5}P_{6,7}, \; P_{3,6}P_{5,7}$
$h_2 - h_5 + h_{11}$	$10g_2 - 5g_5 + g_7$	$P_{1,2}P_{4,5}, \; P_{1,2}P_{4,6}, \; P_{1,3}P_{4,5}, \; P_{1,3}P_{4,7}, \; P_{1,4}P_{5,6}, \; P_{1,4}P_{5,7},$ $P_{2,3}P_{4,6}, \; P_{2,3}P_{4,7}, \; P_{2,4}P_{5,6}, \; P_{2,4}P_{6,7}, \; P_{3,4}P_{5,7}, \; P_{3,4}P_{6,7}$
h_{17}	$-g_1 + 4g_2 + 3g_3 - 6g_4 - g_5$	$P_{1,4}P_{2,5}, \; P_{1,4}P_{3,5}, \; P_{1,6}P_{2,4}, \; P_{1,6}P_{4,5}, \; P_{1,7}P_{3,4}, \; P_{1,7}P_{4,5},$ $P_{2,4}P_{3,6}, \; P_{2,5}P_{4,6}, \; P_{2,7}P_{3,4}, \; P_{2,7}P_{4,6}, \; P_{3,5}P_{4,7}, \; P_{3,6}P_{4,7}$
h_{17}	$-g_1 + 4g_2 + 3g_3 - 6g_4 - g_5$	$P_{1,4}P_{2,6}, \; P_{1,4}P_{3,7}, \; P_{1,5}P_{2,4}, \; P_{1,5}P_{3,4}, \; P_{1,5}P_{4,6}, \; P_{1,5}P_{4,7},$ $P_{2,4}P_{3,7}, \; P_{2,6}P_{3,4}, \; P_{2,6}P_{4,5}, \; P_{2,6}P_{4,7}, \; P_{3,7}P_{4,5}, \; P_{3,7}P_{4,6}$
$-h_2 + h_5 + h_{17}$	$-g_1 - 6g_2 + 3g_3 - 6g_4 + 4g_5$	$P_{1,4}P_{2,7}, \; P_{1,4}P_{3,6}, \; P_{1,6}P_{3,4}, \; P_{1,6}P_{4,7}, \; P_{1,7}P_{2,4}, \; P_{1,7}P_{4,6},$ $P_{2,4}P_{3,5}, \; P_{2,5}P_{3,4}, \; P_{2,5}P_{4,7}, \; P_{2,7}P_{4,5}, \; P_{3,5}P_{4,6}, \; P_{3,6}P_{4,5}$

Table 2.3: The determined parameters after applying the $[\mathcal{H}_{\mathrm{motif}}, \mathcal{P}] = 0$ and $\mathcal{H}_{\mathrm{motif}} |\psi\rangle = 0$ conditions.

The problem of diagonalizing the Hamiltonian is that we have a 128-dimensional matrix, with 7 independent parameters, and we need the general solution for the eigenstates. Direct diagonalization of a 128×128 matrix with the parameters g_i is a formidable task even for `Mathematica`. To circumvent this difficulty, we use the following trick. We generate random integers for the parameters and take the numerical eigenvectors of the Hamiltonian. Then the tensor product of the Hamiltonian and the numerical eigenvectors, and them transpose ($\{\mathbf{n}_i\} \otimes H \otimes \{\mathbf{n}_i\}^{\mathrm{T}}$, where $\mathbf{n}_i$ is the i. numerical eigenvector) gives back the partly diagonalized Hamiltonian. Then we take those elements of the diagonal,

which contains numbers that are integers. Repeating it several times, we can identify 104 eigenvalues of the Hamiltonian.

Degeneracy	Eigenvalue
32	0
4	$-90g_2 + 30g_3 + 60g_5$
4	$9g_1 - 36g_2 + 48g_3 - 66g_4 + 54g_5 + 9g_6$
6	$-14g_1 - 119g_2 - 58g_3 + 81g_4 + g_5 + 9g_6 - 3g_7$
2	$12g_1 - 33g_2 + 54g_3 - 33g_4 + 27g_5 + 9g_6 + 3g_7$
12	$-14g_1 + 91g_2 + 47g_3 - 39g_4 - 29g_5 + 6g_7$
8	$6g_1 + 51g_2 + 27g_3 - 39g_4 - 9g_5 + 6g_7$
8	$6g_1 + 6g_2 + 12g_3 + 6g_4 + 6g_5 + 6g_7$
12	$-14g_1 + 11g_2 + 47g_3 - 39g_4 + 11g_5 + 6g_7$
2	$18g_1 - 27g_2 + 6g_3 + 93g_4 - 27g_5 + 9g_6 + 9g_7$
6	$4g_1 + 59g_2 + 38g_3 - 21g_4 - g_5 + 9g_6 + 15g_7$
8	$-63g_1 + 42g_2 + 54g_3 - 108g_4 - 48g_5 + 9g_6 + 18g_7$

Table 2.4: The determined eigenvalues with their degeneracy.

To determine the remaining 24 eigenvalues, we calculated the S_z operator, and added it to the Hamiltonian with a small weight: $H + \delta S_z$, where δ is a small number. Next, we generated random integers for the parameters and diagonalized the matrix. Then choosing the eigenvectors for which the $\langle \mathbf{v}_i | S_z | \mathbf{v}_i \rangle$ is non-zero, we get 4×6 eigenvectors, with S_z equal $-3/2, -1/2, 1/2, 3/2$. With these, the Hamiltonian will have the same eigenvalues for all S_z. Then, it is enough to determine the eigenvalues for just one case of S_z. The tensor product of the Hamiltonian and the eigenvectors, with $S_z = 3/2$, and their transpose ($\{\mathbf{v}_i\} \otimes H \otimes \{\mathbf{v}_i\}^{\mathrm{T}}$, where $\mathbf{v}_i$ is the i-th eigenvector, with $S_z = 3/2$), gives a 6×6 matrix, whose eigenvalues can be determined by characteristic polynomial method. The results can be seen in Tab. 2.2.

Degeneracy	Eigenvalue
2×4	$\frac{1}{2}(21g_1 + 126g_2 + 42g_3 + 66g_4 - 54g_5 + 9g_6 + 12g_7 \pm \sqrt{(-21g_1 - 126g_2 - 42g_3 - 66g_4 + 54g_5 - 9g_6 - 12g_7)^2 - } $ $-4(2310g_1g_2 - 6240g_2^2 + 630g_1g_3 + 1800g_2g_3 + 360g_3^2 + 7260g_2g_4 + 1980g_3g_4 - 840g_1g_5 + 5820g_2g_5 - 900g_3g_5 - $ $-2640g_4g_5 - 1440g_5^2 + 990g_2g_6 + 270g_3g_6 - 360g_5g_6 + 1320g_2g_7 + 360g_3g_7 - 480g_5g_7))$
2×8	$\frac{1}{2}(6g_1 + 96g_2 + 42g_3 + 6g_4 - 24g_5 + 6g_7 \pm \sqrt{(-6g_1 - 96g_2 - 42g_3 - 6g_4 + 24g_5 - 6g_7)^2 - }$ $-4(-7140g_2^2 + 60g_1g_2 + 360g_3^2 + 180g_1g_3 + 2700g_2g_3 + 60g_2g_4 + 180g_3g_4 - 2340g_5^2 + 60g_1g_5 + $ $+8520g_2g_5 - 900g_3g_5 + 60g_4g_5 + 60g_2g_7 + 180g_3g_7 + 60g_5g_7))$

Table 2.5: The remaining 24 eigenvalues and their degeneracy.

Now we are in a position to satisfy the positivity of the eigenvalues. We are searching for one parameter solutions for simplicity. Since we can fix a parameter, we select g_3 to be

1. We got several solutions for our requirements, and we chose the one with the least terms. It can be seen in Eq. (2.14). The g parameter should satisfy the $g > 35/18$ condition.

$$
\begin{aligned}
\mathcal{H}^{\mathrm{motif}} =& 5(P_{1,2} + P_{1,3} + P_{2,3} + P_{5,6} + P_{5,7} + P_{6,7} + P_{1,4} + P_{2,4} + P_{3,4} + P_{4,5} + P_{4,6} + P_{4,7}) \\
&+ g(P_{1,2}P_{6,7} + P_{1,3}P_{5,6} + P_{2,3}P_{5,7} + P_{1,2}P_{5,6} + P_{1,2}P_{5,7} + P_{1,3}P_{5,7} + P_{1,3}P_{6,7} \\
&+ P_{2,3}P_{5,6} + P_{2,3}P_{6,7}) \\
&- \frac{5}{2}(P_{1,2}P_{3,4} + P_{1,3}P_{2,4} + P_{1,4}P_{2,3} + P_{4,5}P_{6,7} + P_{4,6}P_{5,7} \\
&+ P_{4,7}P_{5,6} + P_{1,2}P_{3,5} + P_{1,3}P_{2,7} + P_{1,6}P_{2,3} + P_{1,6}P_{5,7} + P_{2,7}P_{5,6} + P_{3,5}P_{6,7} \\
&+ P_{1,2}P_{3,6} + P_{1,2}P_{3,7} + P_{1,3}P_{2,5} + P_{1,3}P_{2,6} + P_{1,5}P_{2,3} + P_{1,5}P_{6,7} + P_{1,7}P_{2,3} \\
&+ P_{1,7}P_{5,6} + P_{2,5}P_{6,7} + P_{2,6}P_{5,7} + P_{3,6}P_{5,7} + P_{3,7}P_{5,6}) \, . \qquad (2.14)
\end{aligned}
$$

2.3   16- and 20- site clusters

In this section, we check the ground state degeneracy of the determined Hamiltonian (Eq. (2.14)) on different sized clusters, since if it gives back the expected degeneracy, it can be used to replace the complicated projector. From Sec. 2.1 it is known that the $|\psi_{\mathrm{A}}\rangle$ ground state is $2^{N_{\mathrm{tet}}/2}$ degenerate, and the same is true for the $|\psi_{\mathrm{B}}\rangle$. Therefore the ground state degeneracy of the pyrochlore lattice formed from N_{tet} corner-sharing tetrahedra is $2 \cdot 2^{N_{\mathrm{tet}}/2}$.

(a)   (b)   (c)
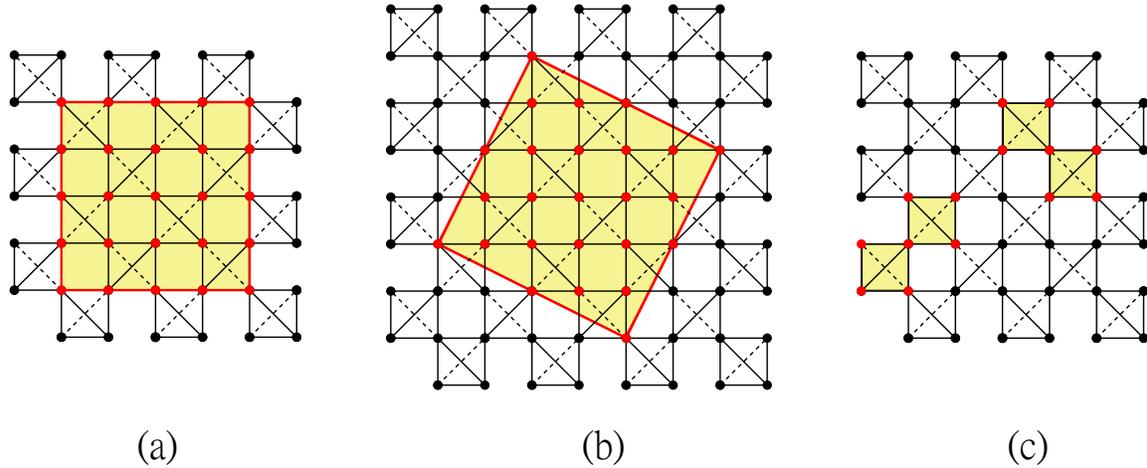
Figure 2.3: The 16- and 20-site cluster in the (a), (b) figure (yellow area delimited by a red line). In the (c) figure, there are two possible coverage of the cluster (yellow area delimited by a red line).

The 2-dimensional representation of the pyrochlore lattice is the well-known checkerboard lattice and, in the following, we will use it to reduce the complexity of the calcu-

lation. We examine the degeneracy on the checkerboard lattice with $N = 16, \ 20$ site clusters as in Fig. 2.3(a) and (b). The lattice vectors for $N = 16$ is $v_1^{(16)} = (0, 4)$ and $v_2^{(16)} = (4, 0)$, for $N = 20$ is $v_1^{(20)} = (2, 4)$ and $v_2^{(20)} = (4, -2)$, which gives the periodic boundary conditions of the cluster. To get the Hamiltonian of the lattice, like in Eq. (2.5), we need to sum the Hamiltonians of all motif on the cluster:

$$\mathcal{H} = \sum_{i=1}^{N} \mathcal{H}_i^{\text{motif}}, \tag{2.15}$$

where the sum runs from 1 to N, since there are N possible ways to embed the motif into the cluster, like in Fig.2.3(c). As we have the $\mathcal{H}^{\text{motif}}$ with permutations indexed by the rule in Fig. 2.1(b), we just need to re-index the $\mathcal{H}^{\text{motif}}$ for all the motifs in the sum. It is done by assigning indexes to the sites, with periodic boundary condition. This allows us to determine the relation between the new and old indexing, so the permutations can be re-indexed too. Having obtained the $\mathcal{H}$ Hamiltonian of the lattice, the ground state can be determined by diagonalizing the matrix representation of the Hamiltonian in the $\binom{N}{N/2}$ dimensional Hilbert-space. We have a 12870×12870 matrix for the 16-site cluster and 184756×184756 for the 20-site cluster, so the full diagonalization is computationally expensive or impossible. Instead, we use the Lánczos-method, which provides the numerically exact m smallest eigenvalues and eigenvectors. This is an iterative method, whose result depends on the input vector. To determine the degeneracy, we initialized the Lánczos-method with random vectors and run it several times, with the hope, that it will span the ground state manifold. For the $N = 16$ cluster, we run it 40 times, and in the case of $N = 20$ run 100 times. The tensor product of this set of eigenvectors and their transpose gives the overlap matrix, whose rank determines the degeneracy. To calculate the rank, we diagonalized the overlap matrix, and count the number of nonzero elements. The calculated eigenvalues of the overlap matrix in the case of $N = 16$ and 20 are displayed in Fig. 2.4 and Fig. 2.5. As we can see, in both cases the degeneracy of the ground state is equal to $2 \cdot 2^{N_{\text{tet}}/2}$. For $N = 16$ the number of tetrahedra is $N_{\text{tet}} = N/2 = 8$ and the dimension of the ground state manifold $\mathcal{M}_{\text{A} \cup \text{B}}$ is $2 \cdot 2^4 = 32$, as the number of the nonzero eigenvalue in Fig. 2.4. For $N = 20$, the degeneration is $2 \cdot 2^5 = 64$ as in Fig. 2.5.
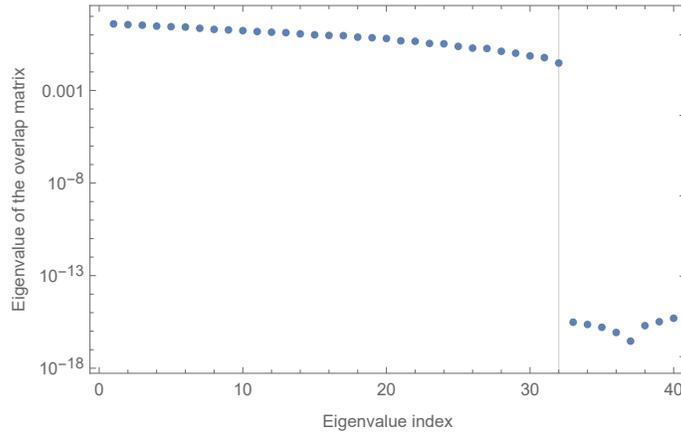
Figure 2.4: The degeneracy of the 16-site cluster with $g = 1$ parameter. The eigenvalues of the overlap matrix is plotted on logarithmic scale. We recover the 32 dimensional $\mathcal{M}_{A \cup B}$ manifold.
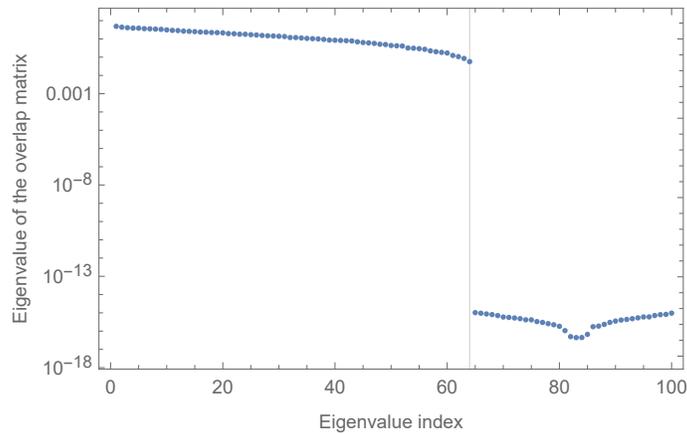

Figure 2.5: The degeneracy of the 20-site cluster with $g = 1$ parameter. The eigenvalues of the overlap matrix is plotted on logarithmic scale. We recover the 64 dimensional $\mathcal{M}_{A \cup B}$ manifold.

Then we examined the ground state of the Hamiltonian. We plot the minimum of the eigenvalues in Figs. 2.6 and 2.7 as a function of parameter g in Eq. (2.14). As we can see, the ground state of the $\mathcal{H}$ Hamiltonian is zero for $g \geqslant 0$, and ferromagnetic when $g < 0$. When we created the $\mathcal{H}^{\text{motif}}$ Hamiltonian of the motif, we required, that the $|\psi\rangle \in \mathcal{M}_{A \cup B}$ should be ground state, but for $g < 35/18$ the energy of a state $|\varphi\rangle \notin \mathcal{M}_{A \cup B}$ become lower than 0, the energy of $|\psi\rangle$. When we consider the energy of $\mathcal{H}$ Hamiltonian of the lattice, it turns out, that the $|\psi\rangle$ wavefunction remains ground states under $g < 35/18$. It is probably because the $|\varphi\rangle$ wavefunction cannot be a simultaneous eigenstate of the

overlapping motifs, which increases the energy of these states so the $|\psi\rangle$ could remain a ground state.
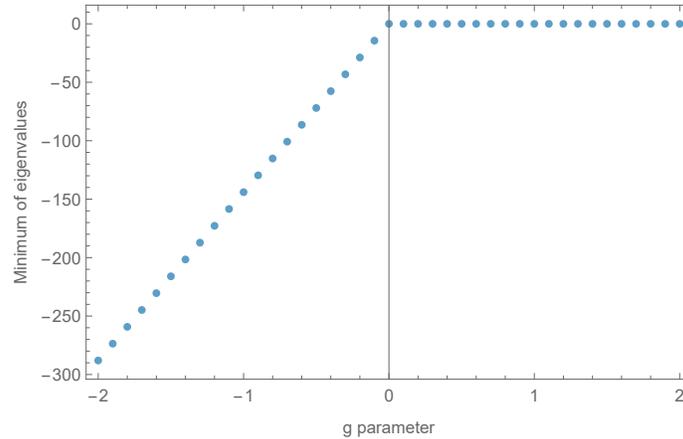

Figure 2.6: The minimum of the of the eigenvalues (blue points) of the Hamiltonian in the 16-site cluster. The parameter g runs from -2 to 2.
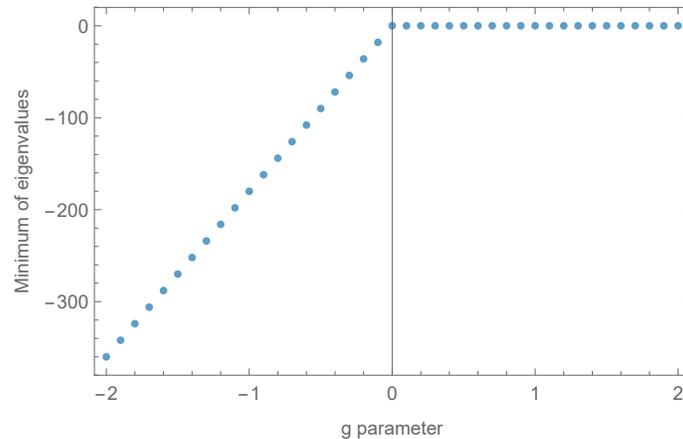

Figure 2.7: The minimum of the of the eigenvalues (blue points) of the Hamiltonian in the 20-site cluster. The parameter g runs from -2 to 2.

2.4 Physically motivated Hamiltonians

The Eq. 2.14 provide us a simple Hamiltonian, which describes the motif, but it is just a mathematical approach, it has no physical meaning. Examining this Hamiltonian, we found an interesting case, when the permutations are taken from two triangles, as in

Fig. 2.8(a).

$$\mathcal{H}_\mathrm{P} = (P_{1,2} + P_{1,3} + P_{2,3})(P_{5,6} + P_{5,7} + P_{6,7}) \tag{2.16a}$$
$$= (S_\mathrm{tot}^{123}(S_\mathrm{tot}^{123} + 1) - 3/4)(S_\mathrm{tot}^{567}(S_\mathrm{tot}^{567} + 1) - 3/4) \tag{2.16b}$$

This Hamiltonian acting on a state from the ground state manifold gives zero since one of the factors in the equation above will act on a singlet on one of the tetrahedra giving zero as in Eq. (1.13).
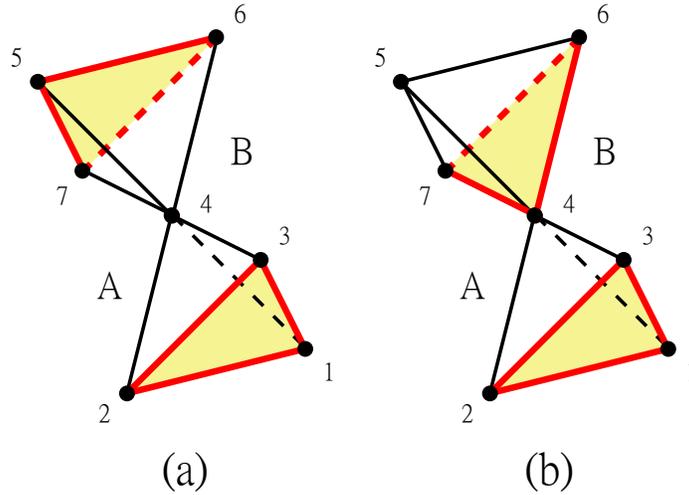

(a) (b)

Figure 2.8: The triangles taking part in the Hamiltonian $\mathcal{H}_\mathrm{P}$ and $\mathcal{H}_\mathrm{Q}^{(123)(467)}$.

Then we examined if there is any other triangle configuration in the motif, which works the similar way as above. Another triangle configuration is pictured in Fig. 2.8(b), with Hamiltonian:

$$\mathcal{H}_\mathrm{Q}^{(123)(467)} = (P_{1,2} + P_{1,3} + P_{2,3})(P_{4,6} + P_{4,7} + P_{6,7}) \,. \tag{2.17}$$

There are 6 possible choices of pair of triangles in the motif. The sum over the symmetry equivalent pair a of triangle, $\mathcal{H}_\mathrm{A}^{(123)(467)} + \mathcal{H}_\mathrm{A}^{(123)(456)} + ...$, divided by 2 for convenience, is

$$\begin{aligned}
\mathcal{H}_\mathrm{Q} &= (P_{1,2} + P_{1,3} + P_{2,3})(P_{4,5} + P_{4,6} + P_{4,7}) \\
&+ (P_{1,2} + P_{1,3} + P_{2,3})(P_{5,6} + P_{5,7} + P_{6,7}) \\
&+ (P_{1,4} + P_{2,4} + P_{3,4})(P_{5,6} + P_{5,7} + P_{6,7}) \,.
\end{aligned} \tag{2.18}$$

Since the $\mathcal{H}_\mathrm{Q}^{(123)(467)} |\psi\rangle = 0$, where $|\psi\rangle \in \mathcal{M}_{\mathrm{A}\cup\mathrm{B}}$, therefore the sum of the equivalent Hamiltonian-s gives zero as well, $\mathcal{H}_\mathrm{Q} |\psi\rangle = 0$.

Furthermore, we noticed, that we can choose g_i parameters in Tab. 2.3, to cancel all the terms containing 4-site exchanges. This Hamiltonian is

$$
\begin{aligned}
\mathcal{H}_{\mathrm{R}} =& P_{1,4} + P_{1,5} + P_{1,6} + P_{1,7} + P_{2,4} + P_{2,5} + P_{2,6} + \\
& + P_{2,7} + P_{3,4} + P_{3,5} + P_{3,6} + P_{3,7} + P_{4,5} + P_{4,6} + P_{4,7} - 6 \\
=& \left[\sum_{1 \leqslant i < j}^{7} P_{i,j} \right] - (P_{1,2} + P_{1,3} + P_{2,3}) - (P_{5,6} + P_{5,7} + P_{6,7}) - 6 \\
=& \, S_{1\dots7}(S_{1\dots7} + 1) - S_{123}(S_{123} + 1) - S_{567}(S_{567} + 1) - \frac{3}{4} \, .
\end{aligned} \tag{2.19}
$$

The problem with the Hamiltonian above, that it has negative eigenvalues. Can we heal this problem, by adding the $\mathcal{H}_P$ and $\mathcal{H}_Q$ to it? We added these Hamiltonians with different parameters

$$
\mathcal{H}^{\mathrm{motif}} = J_p \mathcal{H}_{\mathrm{P}} + J_q \mathcal{H}_{\mathrm{Q}} + J_r \mathcal{H}_{\mathrm{R}}. \tag{2.20}
$$

The eigenvalues of this Hamiltonian are collected in Tab. 2.6.

S_{tot}	E	degeneracy
	0	8*
1/2	$-3J_r + 6J_q$	4
	$-6J_r + 12J_q + 9J_p$	1
	$-6J_r + 18J_q + 9J_p$	1
	0	4*
	$3J_r$	4
3/2	$6J_q$	4
	$-3J_r + 9J_q + 9J_p$	1
	$-3J_r + 21J_q + 9J_p$	1
	$5J_r + 6J_q$	4
5/2	$2J_r + 6J_q + 9J_p$	1
	$2J_r + 24J_q + 9J_p$	1
7/2	$9J_r + 27J_q + 9J_p$	1

Table 2.6: Energies and degeneracies of the $\mathcal{H}^{\mathrm{motif}} = J_p \mathcal{H}_{\mathrm{P}} + J_q \mathcal{H}_{\mathrm{Q}} + J_r \mathcal{H}_{\mathrm{R}}$. The total angular momentum S_{tot} of the eigenstates is given in the first column. The star denotes the $2 \times 8 + 4 \times 4 = 32$ eigenstates in the $\mathcal{M}^{\mathrm{motif}}_{A \cup B}$ manifold.

The energies are all non-negative for $J_r \geqslant 0$ only, so we can set the energy scale by $J_r = 1$. Then the condition for all the energies to be positive is

$$\left(J_p \leqslant -\frac{4}{3} \wedge J_q \geqslant -\frac{3J_p}{2} - \frac{1}{3}\right) \vee \left(-\frac{4}{3} < J_p \leqslant -\frac{2}{3} \wedge J_q \geqslant \frac{1}{3} - J_p\right) \vee$$
$$\vee \left(-\frac{2}{3} < J_p \leqslant 0 \wedge J_q \geqslant \frac{1}{2} - \frac{3J_p}{4}\right) \vee \left(0 < J_p \wedge J_q \geqslant \frac{1}{2}\right) \tag{2.21}$$

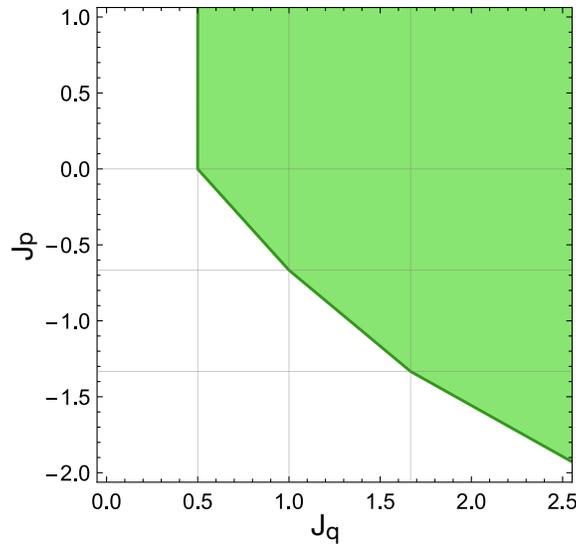The region of allowed J_r and J_p is shown in Fig. 2.9.

Figure 2.9: The region (green area) of the possible J_p, J_q parameters, with fixed $J_r = 1$. The paremeters in this area satisfies the positivity of the energies of the $\mathcal{H}^{\mathrm{motif}} = J_p\mathcal{H}_{\mathrm{P}} + J_q\mathcal{H}_{\mathrm{Q}} + J_r\mathcal{H}_{\mathrm{R}}$ Hamiltonian.

In the followings, we choose $J_p = 0$, $J_r = 1$ and vary the J_q parameter only. We checked the degeneracy of the ground state for $J_q = 1$ on a 20-site cluster with the same method discussed in Sec. 2.3. We got the expected 64 ground states. The ground state energy as a function of J_q can be seen in Fig. 2.10. For $J_q \gtrsim 0.175$ the $\mathcal{M}_{\mathrm{A \cup B}}$ manifold is the ground state. This value is again smaller than $J_q = 0.5$ anticipated by the eigenvalues of the motif, as in Fig. 2.9. For $J_q \lesssim -0.6$ the ground state is the ferromagnet. Among these values, the ground states are other states. This is a very encouraging result because we found a Hamiltonian, where the weight of the 4-site exchanges is relatively small. In realistic models, the 4-site exchanges are higher-order processes, whose strengths are weaker than those of the 2-site exchanges.
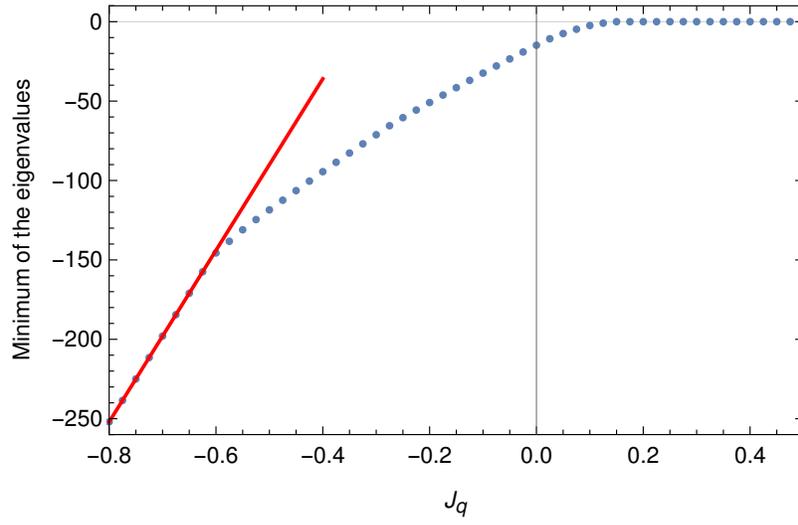
Figure 2.10: The ground state energy as a function of the J_q, where $J_p = 0$ and $J_r = 1$, examined on the 20-site cluster. The blue points denote the ground state energies and the red line the energy of the ferromagnetic state.

Chapter 3

Summary and outlook

The quantum spin models on frustrated lattices are among the most complex problems in modern condensed matter physics. Especially in higher dimensions, the theoretical approach is often limited to numerical methods. Here we investigated spins on the highly frustrated pyrochlore lattice in the extreme quantum limit. The goal of our research was to engineer Hamiltonians where the ground states are known exactly. These Hamiltonians are involved, but we hope they may serve as a starting point for a better understanding of the phases in these models.

A recent numerical calculation suggested a possible inversion symmetry breaking phase in the pyrochlore lattice. This inspired us to construct a Hamiltonian with exact ground states which spontaneously break this symmetry and consists of spins forming singlets on a sublattice of tetrahedra. This ground state not only breaks inversion symmetry but is also extensively degenerate forming a manifold. In the spirit of the Majumdar-Ghosh model, we created a Hamiltonian as a sum of projectors with the sought-after ground state manifold. The projectors are defined on a motif consisting of 7 sites forming two corner-sharing tetrahedra. These motifs give a full covering of the lattice. The projector consists of many terms, including 6-site exchanges.

To find a simpler Hamiltonian, we considered a linear combination of the two- and four-site exchanges on the motif. We required the ground state manifold to have zero energy, and all other states to have finite positive energies. Using this mathematical construction, we arrived to a set of Hamiltonians satisfying the required conditions. To check the validity of our approach, we considered our Hamiltonian on 16- and 20-site clusters with periodic boundary conditions. Numerical exact diagonalization confirmed the anticipated degeneracy of the ground state manifold. Examination of the structure of the solution, we found a transparent and physically motivated method to construct Hamiltonians with the desired property. In the end, we arrived at a relatively simple form, the Hamiltonian on the motif consisted only of two- and four-site exchanges which are a product of permutations on non-overlapping triangles. Exact diagonalization revealed that the weight of the four-site exchange can be relatively small compared to two-site exchanges.

The final result raised the question of whether such four-site exchanges can be realized in a physical system. For example, the magnetoelastic coupling can give four-site exchanges, also fluctuations can effectively be described by higher-order terms.

Another question is how does the extensive ground state manifold lift its degeneracy.

The model we got is likely describing a quantum critical point, where many phases meet. Departing from this point will introduce different effective interactions among the degrees of freedom of the singlets on the tetrahedra. These are, however, studies left for the future.

Acknowledgments

Appendix

Here we give an expression relating the sum of $P_{i,j}$ over an N-site complete graph to the total spin S_N:

$$
\begin{aligned}
\sum_{i=1}^{N-1}\sum_{j=i+1}^{N} P_{i,j} &= \sum_{i=1}^{N-1}\sum_{j=i+1}^{N} 2\,\mathbf{S}_i \cdot \mathbf{S}_j + \frac{1}{2}\frac{N(N-1)}{2} \\
&= \left(\sum_{i=1}^{N} \mathbf{S}_i\right)^2 - N\mathbf{S}_i^2 + \frac{N(N-1)}{4} \\
&= \left(\sum_{i=1}^{N} \mathbf{S}_i\right)^2 - N\frac{3}{4} + \frac{N(N-1)}{4} \\
&= S_N(S_N+1) + \frac{N(N-4)}{4}\ .
\end{aligned}
\tag{3.1}
$$

Bibliography

[1] I. Hagymási, R. Schäfer, R. Moessner, and D. J. Luitz, "Possible inversion symmetry breaking in the $s = 1/2$ pyrochlore heisenberg magnet," *Phys. Rev. Lett.*, vol. 126, p. 117204, Mar 2021. [Online]. Available: https://link.aps.org/doi/10.1103/PhysRevLett.126.117204

[2] P. Fazekas, *Lecture notes on electron correlation and magnetism*, ser. Series in Modern Condensed Matter Physics: Volume 5.   World Scientific, 1999.

[3] H. Takagi and S. Niitaka, *Highly Frustrated Magnetism in Spinels*.   Berlin, Heidelberg: Springer Berlin Heidelberg, 2011, pp. 155–175. [Online]. Available: https://doi.org/10.1007/978-3-642-10589-0_7

[4] J. T. Chalker, *Geometrically Frustrated Antiferromagnets: Statistical Mechanics and Dynamics*.   Berlin, Heidelberg: Springer Berlin Heidelberg, 2011, pp. 3–22. [Online]. Available: https://doi.org/10.1007/978-3-642-10589-0_1

[5] R. Moessner and J. T. Chalker, "Low-temperature properties of classical geometrically frustrated antiferromagnets," *Phys. Rev. B*, vol. 58, pp. 12049–12062, Nov 1998. [Online]. Available: https://link.aps.org/doi/10.1103/PhysRevB.58.12049

[6] K. W. Plumb, H. J. Changlani, A. Scheie, S. Zhang, J. W. Krizan, J. A. Rodriguez-Rivera, Y. Qiu, B. Winn, R. J. Cava, and C. L. Broholm, "Continuum of quantum fluctuations in a three-dimensional S = 1 Heisenberg magnet," *Nature Physics*, vol. 15, no. 1, pp. 54–59, Jan. 2019.

[7] Y. Yamashita and K. Ueda, "Spin-driven jahn-teller distortion in a pyrochlore system," *Phys. Rev. Lett.*, vol. 85, pp. 4960–4963, Dec 2000. [Online]. Available: https://link.aps.org/doi/10.1103/PhysRevLett.85.4960

[8] H. Bethe, "Zur Theorie der Metalle," *Zeitschrift fur Physik*, vol. 71, no. 3-4, pp. 205–226, Mar. 1931.

[9] F. D. M. Haldane, "Spontaneous dimerization in the $s = \frac{1}{2}$ heisenberg antiferromagnetic chain with competing interactions," *Phys. Rev. B*, vol. 25, pp. 4925–4928, Apr 1982. [Online]. Available: https://link.aps.org/doi/10.1103/PhysRevB.25.4925

[10] Y. Iqbal, T. Müller, P. Ghosh, M. J. P. Gingras, H. O. Jeschke, S. Rachel, J. Reuther, and R. Thomale, "Quantum and classical phases of the pyrochlore heisenberg model with competing interactions," *Phys. Rev. X*, vol. 9, p. 011005, Jan 2019. [Online]. Available: https://link.aps.org/doi/10.1103/PhysRevX.9.011005

[11] H. Tsunetsugu, "Spin-singlet order in a pyrochlore antiferromagnet," *Phys. Rev. B*, vol. 65, p. 024415, Dec 2001. [Online]. Available: https://link.aps.org/doi/10.1103/PhysRevB.65.024415